IN-SITU TERRAIN ANALYSIS FOR PLANETARY ROVERS

Gabrielle Hedrick[a], Dylan Covell[a], Yu Gu[a]

[a] *Department of Mechanical and Aerospace Engineering, 1306 Evansdale Drive, PO Box 6106 Morgantown, West Virginia 26506-6106*
glc0006@mix.wvu.edu, dmcovell@mix.wvu.edu, yu.gu@mail.wvu.edu

Abstract

NASA is proposing a Mars Sample Return mission to bring back material from Mars, proposed to be completed in 100 to 200 Martian days (or sols). Due to landing uncertainty, the rover would potentially need to cover distances up to 10 km to collect the samples. Recent surface missions have been limited in their driving capabilities, such as drive time and distances covered, due to a variety of factors including lack of autonomy and communication with Earth, and uncertainty about the environment. To increase drive time, it is crucial to integrate methods to gain information about the terrain into the path planning process and facilitate traversability assessments. This paper presents a rover-mounted instrument capable of obtaining good knowledge of the terrain by measuring the in-situ parameters cohesion c and angle of internal friction ϕ. The instrument selected is a pocket shear vane, that gives shear stresses for given normal stresses. They are then used to compute the Mohr-Coulomb failure criterion from which the terrain parameters are derived. It is adapted to be mounted on a rover and controlled remotely, with a capability of generating stresses up to almost 400 kPa. Tests are conducted on reference soils in the laboratory as well as in-situ, with the instrument mounted on linear guide rails, and results obtained are close to the expected parameters of each soil tested. The main contributions of this work are: 1) to provide a planetary surface rover an easy option to gather intrinsic soil parameters that can be used to identify a terrain when needed; 2) to provide a method to identify a terrain with little to no human intervention; 3) to obtain results in a timely manner (a few minutes per measurement) to allow a fast traverse rover to quickly make a decision regarding its path given the terrain characteristics.

Keywords: Mars Rover, Shear Vane, Cohesion, Angle of Internal Friction

1. Introduction

Space missions are becoming increasingly complex, as shown by the proposed Mars Sample Return (MSR) mission (Witze, 2014) to be completed in a shorter amount of time than previous surface mission. Such a mission requires enhanced autonomy compared to current surface robots, to enable further and faster driving than existing Mars rovers, with limited communication.

The next journey to Mars is a proposed fetch rover to gather and bring back samples collected by Perseverance. The sample return proposal brings a new level of complexity to engineers: it is mostly designed to bring back samples (vs. performing science experiments), unlike any other missions to the red planet, and is planned to be completed in less than one Martian year (687 Martian days or sols) (MEPAG, 2008). The landing ellipse for the Perseverance rover is roughly 11 km by 8 km (Golombek et al., 2017), and assuming a similar landing area for MSR, the fetch rover might have to traverse potentially great distances in a short amount of time. A similar sized rover such as Opportunity drove an average of 3 km in 1 Earth year (Schroeder, 2019) with the designed capability of driving four hours in one sol (Biesiadecki et al., 2007). Therefore, MSR calls for more autonomy beyond the pre-planning done by humans.

To understand better how autonomy is becoming a necessary part of NASA's future missions, it is important to know how the past and current Mars missions are organized in terms of daily planning. A typical sol (about 40 minutes longer than a day on Earth) includes one downlink and one uplink through the Deep Space Network (DSN), which means that Earth communicates with the rover only a couple of times a day (Bajracharya et al., 2008). The downlink provides the team with images and other results from the previous sols that they can use to navigate, and rover movements are therefore limited to line-of-sight driving. There is an autonomous navigation feature, "AutoNav", that allows the rover planners to drive beyond what is seen on images, but it is very slow - for MER, speeds could drop down to 10 m/hr (Biesiadecki et al., 2007). Moreover, driving is not scheduled every sol (Gaines et al., 2016) resulting in overall speed and distances covered not adequate for MSR.

Hence, there is a need for increased autonomous driving distance due to the potential size of the landing ellipse and the plan for a duration of only about 100 to 200 Martian sols (i.e., Martian days) for the MSR mission (Klein et al., 2014). To increase driving distances and go beyond line-of-sight from downlinked images, it is necessary to know the terrain and assess its traversability, i.e., its ability to sustain a driving robot without reaching failure (Papadakis, 2013). Some research has already been performed regarding a terrain-aware path planning that efficiently takes into consideration terrain information as the rover drives (Hedrick et al., 2020). This work focuses on a method to gather in-situ information about the terrain that can be utilized in the aforementioned path planning, and significantly lower the uncertainty related to traversability. The main idea is to support the prediction of performance on the terrain ahead and help the rover make adequate decisions regarding its path using reliable information about the soil obtained from in-situ measurements.

This paper is organized as follows: after presenting relevant research, a problem statement and contributions will be detailed. This section will be followed by the technical approach, results of this work, and finally the conclusion.

2. Related Work

Planetary surface exploration is challenging for many reasons, including the lack of knowledge about the soil. A lot of work has been dedicated to modeling terrains in order to improve rover performance during such missions, ranging from remote sensing (such as thermal inertia, radar, optical methods, etc...) to in-situ analysis of terrain, directly or indirectly (such as rover sub-systems, instrumentation, etc...) (Chhaniyara et al., 2012).

One important approach to traversability analysis involves terramechanics, i.e., the study of the interaction between the wheels and the soil. Vibrations induced by the terrain interacting with the wheels during driving has been suggested as a mean to classify terrains (Brooks & Iagnemma, 2005). Wheel slip, torque, sinkage and drawbar pull are among the parameters suggested to sense the terrain (Iagnemma et al., 2003). More research was done towards planetary exploration in subsequent years to improve on autonomy and include terrain analysis into path planning, such as computing a path, then evaluating the terrain based on wheel/ground interaction, and finally recomputing the path if necessary (Ishigami et al., 2007). It was later suggested to integrate a full dynamic model of the robot into the path planning, comprising of a sub-model of the vehicle to get a mobility profile, and a terramechanics sub-model to obtain interaction forces on deformable soils. The research proposes to compute several feasible paths, run a dynamic simulation for each candidate and calculate a dynamic mobility index, comprised of roll, pitch, slip, elapsed time and energy required to reach a position (Ishigami et al., 2011).

Another approach involves the use of sensors and cameras to analyze the terrain: for example, using on-board sensors such as gyros, accelerometers, encoders, motor current, voltage, ultra-sonic or infrared sensors, the data are fed into neural networks that characterize and classify the terrain between five different options (gravel, sand, asphalt, grass and dirt) (Ojeda et al., 2006). Similarly, another model suggests using on-board cameras to remotely classify terrains and predict slip. The terrains are then divided into three main categories related to mobility performance: traversable, not traversable, and uncertain. This system has been specifically intended for planetary rovers after seeing the difficulties encountered on Mars (Helmick et al., 2008). Research has also been done towards making the rover a more autonomous explorer, gathering valuable scientific information autonomously and utilizing it to navigate (Girdhar & Dudek, 2016). The idea to use instruments to gain information about the terrain had already been suggested (Chhaniyara et al., 2012), with the study of several hand-held instruments (e.g., cone penetrometers, shear vanes) as potential candidates for astronauts or rovers (Rahmatian & Metzger, 2010). It was found that a modified shear vane could acquire good insight into the soil strength. A similar instrument, called a cone-vane penetrometer was actually used on the Lunakhod rover to estimate the bearing capacity of the soil (Zacny et al., 2010) but did not make any diagnosis regarding other properties such as soil strength. A recent article proposed to integrate a more complex instrument, a spectrometer, to collect information to support rover path planning. In this scenario, the initial map is a belief map of geological units assessed by scientists (potential hypothesis about the soil). The rover updates its route as it is gaining information about the terrain (obtained from the spectrometer) through Bayesian inference (Candela et al., 2017). This paper was inspired by previous work on incorporating Bayesian processes to make planetary rovers more independent in their scientific exploration (Arora et al., 2017). However, the drawback of this method is the cost of using such an instrument (about three hours each time (Gellert et al., 2009), not counting the energy expenditure), and if it is well adapted for scientific mission, it might not be adequate for missions such as the sample return rover.

Finally, a third approach to traversability analysis worth mentioning is the use of orbital imagery. Recently, several authors have looked into predicting traverse performance by taking into account orbital data such as HiRISE (High Resolution Imaging Science Experiment) or slope in a software called Mars Terrain Traversability Tool (Ono et al., 2016). MTTT uses a terrain classifier, Soil Property and Object Classification (SPOC) that analyses HiRISE images to classify different terrains into categories (Rothrock et al., 2016). These terrain types are coupled with rock abundance (Cumulative Fractional Area (Golombek & Rapp, 1996) or CFA), hazards and slope to predict rover speed (Ono et al., 2016). However, the SPOC classifier used in MTTT has a small chance to misclassify the terrains (Rothrock et al., 2016) and the rover would need to account for such scenarios, e.g., by using terramechanics and/or instrumentation to analyze the terrain directly from the surface.

3. Problem statement and contribution

The objective of this work is to equip a rover with the capability of gathering in-situ terrain information at an accuracy equal to or greater than a human operator to support autonomous path assessment and planning. It would allow the vehicle to make decisions regarding its traverse before mobility difficulties could be encountered, by choosing strategic locations to gather meaningful information about the environment. This new knowledge would be used to update the map of the landing site via extrapolation techniques as proposed in Hedrick et al. (2020) and would be a useful input for local planning and replanning along the remaining route. The main constraint is to have human operated experiments widely utilized on Earth adapted to function autonomously on a rover. That is, any hand-held tool needs to be mounted on the rover, and any experiments must be performed remotely. An important assumption is that there is no significant difference between Earth and Mars, meaning, an instrument on Earth and its manipulation on a given terrain will result in similar conclusions when operated on Mars on a similar soil. For example, a cone penetration test on sand is interpreted in the same manner on both planets and results are thus assumed to be valid when carried out on Mars.

The main contributions of this work are the following: 1) to provide an easy option to gather intrinsic soil parameters that can be used to identify a terrain when needed; 2) to give a way of identifying a terrain with little to no human intervention; 3) to obtain results in a timely manner (i.e., a few minutes) to allow a fast traverse rover to quickly make a decision regarding its path given the terrain characteristics.

4. Soil parameters

Cohesion c and angle of internal friction, ϕ characterize soil strength, and are both intrinsic properties of the terrain. Cohesion is the ability for a material to hold itself together and corresponds to the cohesive strength of a terrain. The angle of internal friction gives an estimate of the friction due to the material itself. For example, a terrain with zero cohesion, such as loose rock debris, will still resist deformation due to friction, unless a stress is applied (Melosh, 2011). These two parameters are extremely important in geology, and can be used to classify planetary materials (Sullivan et al., 2011). They also matter in engineering as they can be utilized to retrieve bearing capacity and soil failure point, two important variables that might need to be estimated in the case of a planetary rover to avoid unexpected collapsing of the soil under the wheels. Cohesion and friction are related to the normal and shear stresses via the following equation:

$$\tau = c + \sigma_n tan\phi \tag{1}$$

where τ is the maximum shear stress the soil can handle, and σ_n is the normal stress. Equation 1 represents the linear approximation of the Mohr-Coulomb failure envelope (Zoback, 2010). The intersection of the Mohr-Coulomb failure with the circle of stresses given by σ_1 (vertical stress) and σ_3 (confining pressure) determines the point of failure. Since this study focuses on only one point along the envelope (the point of failure), the linearization is an acceptable approximation (Labuz & Zang, 2012). For a driving rover, assumptions can be made that σ_3 is negligible and σ_1 is the load of the vehicle (Sullivan et al., 2011). The

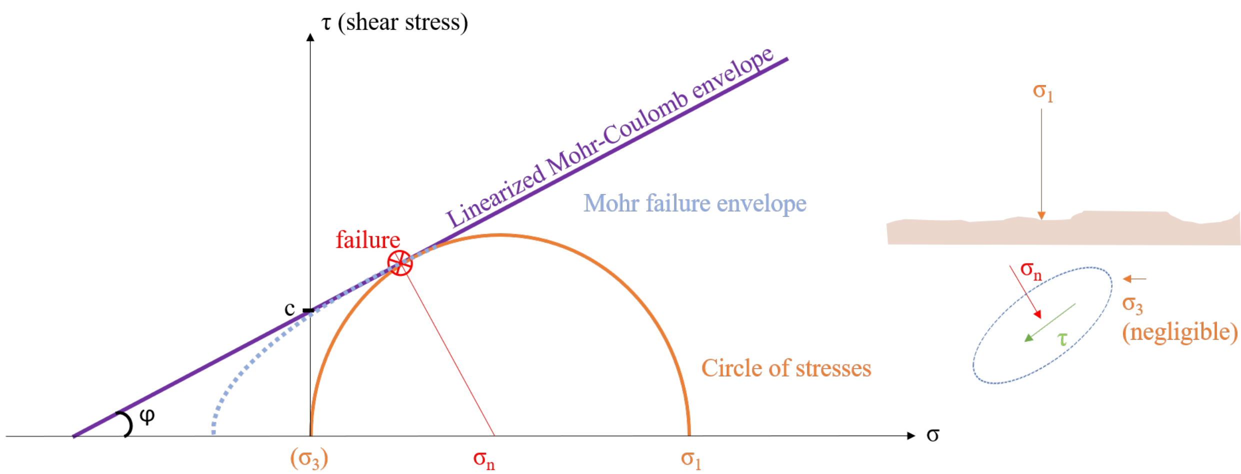

Fig. 1: *Mohr-Coulomb envelope and failure point shown for a vertical load (σ_1) on a terrain. The confining pressure is negligible.*

line perpendicular to the point of failure and intersecting the x-axis gives σ_n. Assuming a known cohesion c and angle of internal friction ϕ, the Mohr-Coulomb failure envelope will give the maximum load (weight, or σ_1) and shear stress (wheel rotation at constant velocity (Sullivan et al., 2011), or τ) a certain planetary terrain can sustain without failing. The concept is illustrated in Fig.1.

5. Technical Approach

5.1. Hand-held pocket shear vane

By knowing selected terrain parameters (i.e., cohesion and friction) and the load of the vehicle, the Mohr-Coulomb curve and circle of stresses can be obtained to find the failure point. There exists direct and indirect methods for measuring these parameters. Direct methods include laboratory testing where samples of soil are subjected to normal stresses and confining pressure (Bishop & Henkel, 1962) in what is called a triaxial test. Indirect methods include shear vane testing, with three main instruments available on the market: the pocket shear vane, the field shear vane and the geovane. Shear testing consists of applying torque to a bladed probe, or vane, until the soil yields (i.e, no resistance is met, when the soil has reached failure). The shear strength value can be read on the instrument dial, with the pointer staying in place when failure occurs (Fig.2).

The amount of required torque varies depending on the blade geometry and depth of testing. The geovane and field vane are lengthy instruments (minimum 30 cm with extension rods available), whereas the pocket shear vane is compact and more applicable to this research, as it will be mounted on a rover. It was therefore chosen as a field instrument for the rover (Fig.2).

Fig. 2: *Pocket Shear Vane Instrument with different blades (optional) (Credit: Gilson inc.)*

However, this instrument gives only the value for shear stress (i.e., τ), while the normal stress is applied by a human operator. As suggested in Rahmatian & Metzger (2010), it can be modified to bear a controlled amount of weight (and therefore, a controlled normal stress can be applied). The modification is shown in Fig.3 and consists of a 3D printed part with slots tailored to calibration weights.

Fig. 3: *Modified pocket shear vane tester including: a 3D printed cast with weight slots; calibration weights.*

The maximum total mass available is 0.55 kg and the minimum is 0.17 kg. By applying different weights to obtain several measurements at the same location, a small range of normal stresses and their associated shear stresses can be plotted. The Mohr-Coulomb envelope can be obtained from these measurements, the resulting slope and y-axis intersection would give ϕ and c, respectively.

5.2. Mounted pocket shear vane

To make the pocket shear vane remotely operable, the human actions must be simplified as electronic motions and the stresses obtained digitally. As seen in Fig.4, the instrument is integrated into an actuated payload equipped with a potentiometer and a pair of identical shear load cells oriented perpendicular to each other.

This prototype was designed with a focus on minimizing undesired skew and payload footprint while remaining simple to manufacture. The T-slot guide rails provide an adaptable means of connecting this sensor to the Fast Traversing Autonomous Rover built at West Virginia University's Interactive Robotics Laboratory. Additionally, the T-slot linear bearings contain no moving parts, an ideal trait for the dusty Martian environment. The linear servos are used over a stepper motor and lead screw to protect from dust and debris.

Once the payload frame is resting on the ground, a linear servo presses down on the shear vane and the resulting normal force is read via the load cell oriented normal to the ground. The output voltage of the load cell is amplified before reaching the arduino. The HX711 library takes this read voltage and outputs an equivalent weight. The rated repeatability of the load cells is +/- 10 g or 0.05% of the maximum range of 20 kg. This value is then converted to a normal stress using Eq.2:

$$\sigma_n = \frac{Wg}{S} \tag{2}$$

Where σ_n is the normal stress, W is the weight of the instrument, g is the gravity ($9.81 m/s^2$ for Earth) and S is the surface area being forced into the soil and covered by the blades (see Fig. 4a). S is specified in the instrument's instruction manual and is equal to $0.000491 m^2$. The measurement from the shear vane is given in kg/cm^2 and converted to kg/m^2. The shear stress is obtained from the measurement simply by multiplying by g.

The resulting shear stress can then be obtained via two methods:

- The potentiometer output, that models the position of the shear vane dial.
- The output of the load cell aligned with the torsional neutral axis is amplified before the arduino reads the voltage. The HX711 library takes this voltage and outputs an equivalent weight, which is then converted to a shear stress using Eq.3:

  $$\tau = \frac{w_m * d * r}{J} \tag{3}$$

  Where τ is the shear stress (Pa), w_m is the measured weight (N), $d = 0.04m$ is the distance between the effective and reactive w_m (the working length of the load cell), $r = 0.00635m$ is the distance between the neutral axis of the load cell and the stressed surface, and $J = 1.10954 \times 10^{-9} m^4$ is the second polar moment of inertia. Therefore, Eq.3 can simply be rewritten as:

  $$\tau = 2.289 \times 10^5 w_m \tag{4}$$

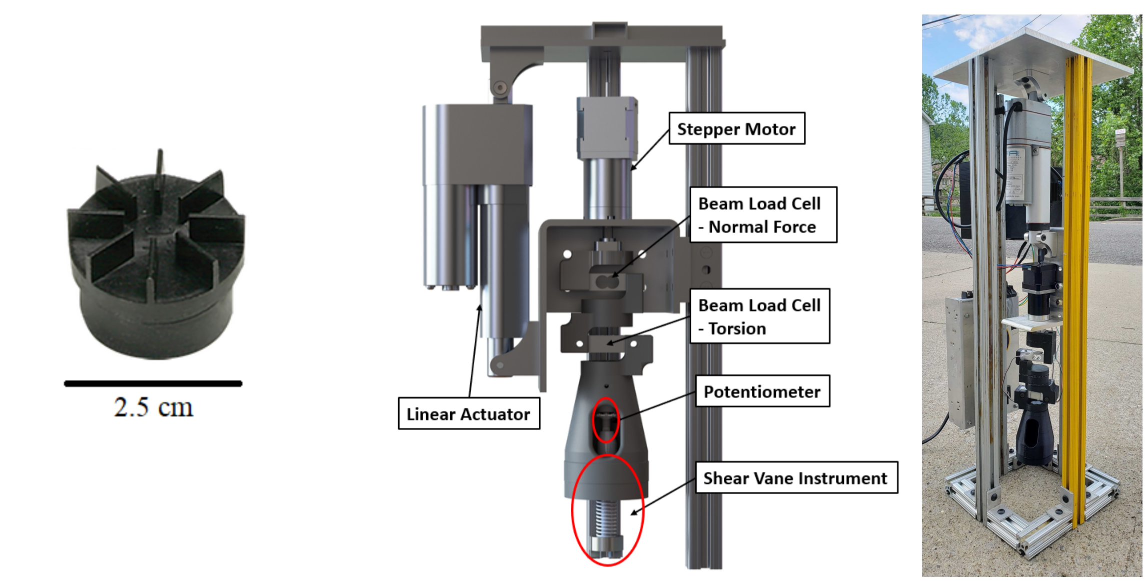

(a) *Pocket shear vane blades used in experiments.*

(b) *Figure of Main Components in Refined Payload*

(c) *Current Physical Prototype (height: 70 cm)*

Fig. 4: *Automated Shear Vane Test Prototype*

This prototype is composed of the electronic hardware found in Table 1 and controlled via MATLAB® through an Arduino Uno. The Arduino library for the load cell amplifier (Giacoboni, 2020) greatly enables a seamless integration of the load cells into MATLAB®.

Table 1: Prototype Hardware and Estimated Maximum Energy Consumption

Component	Maximum Power Consumption (Watts)	Company
Arduino Uno R3	2.5	Arduino
CTS 282T33L502A26C2 Potentiometer	0.005	Digi-Key
FA-PO-150-12-2 Linear Actuator	60	Firgelli Automation
High Current DC Motor Driver	0.08	Firgelli Automation
667oz-in NEMA-17 Stepper Motor	20.4	Phidgets
CZL635 20 kg Load Cell	0.025	Phidgets
DRV8825 Stepper Motor Driver	0.005	Pololu
HX711 Load Cell Amplifier	0.008	Sparkfun

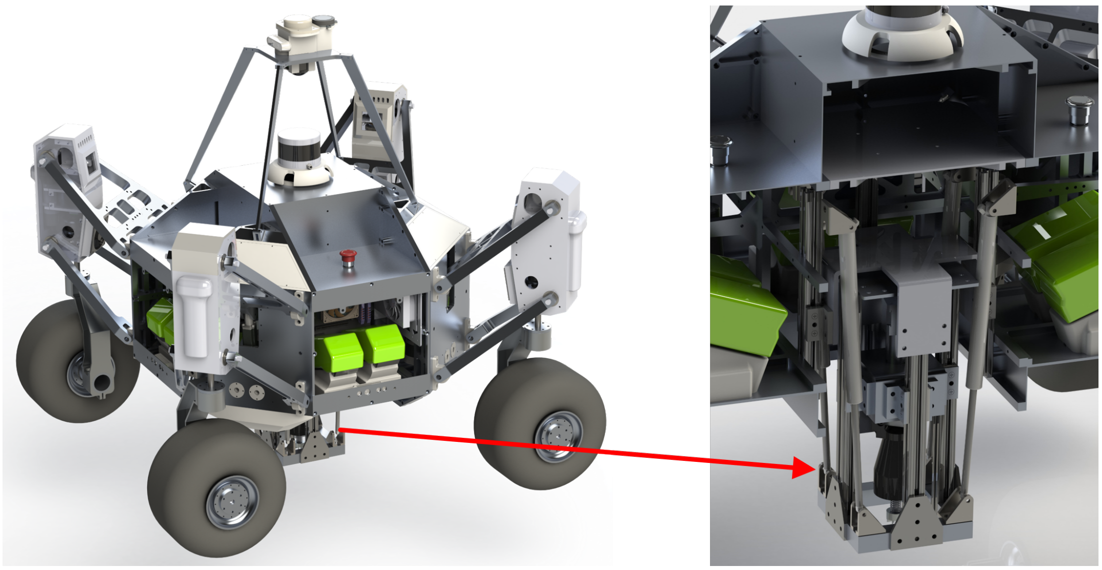

Fig. 5: *mounted pocket shear vane Device inside Fast Traverse Rover*

The first prototype of the refined payload shown inside the center rover compartment (Fig.5) is currently estimated to weigh 7.3 kg and take up a 39.4 cm tall x 16.8 cm wide x 22.9 cm deep box.

6. Results

The modified pocket shear vane was tested in known soils (per United Soil Classification System, or USCS), referred to as controlled samples, to verify that the modifications would lead to adequate results from which cohesion and angle of internal friction could be retrieved (i.e, Mohr-Coulomb envelopes). Several tests were run for each load for each sample (five per controlled sample), and a Mohr-Coulomb type curve fit to the results before being linearized to compute the intrinsic parameters. The loads are obtain for masses ranging from 0.176 g to 0.546 g. The initial curve to be linearized is a power equation of the form:

$$\tau = a\sigma_n^b + c \tag{5}$$

Where τ is the shear stress, σ_n is the normal stress, and a, b, c are constants defining the curve. The linearization is performed by fitting a tangent to the curve after it has flattens.

The tested soils are the following (the official United Soil Classification System (USCS) label is specified for each one):

- Fine sand (USCS SW, SP)
- Clay of low plasticity (USCS CL)
- Silt loam, compacted (USCS ML, OL, MH, OH)

The instrument was then tested in different soils the field with only one to three sets of data per load, to stay as close as possible to the conditions it would operate in when deployed on Mars. The following terrains (estimated by human operators) were tested:

- Silt loam, saturated (USCS ML, OL, MH, OH)
- Sand (USCS SW, SP)

The normal stress is obtained from the range of weights available, using Eq.2. Certain data points were eliminated due to the inadequacy of the testing conditions.

6.1. Hand-held pocket shear vane: controlled samples

Dry clay is of low plasticity, with an expected cohesion of $86kPa$ when compacted, and an angle of internal friction between 27°and 35°. The tests results for compacted dry clay are presented in Fig.6.

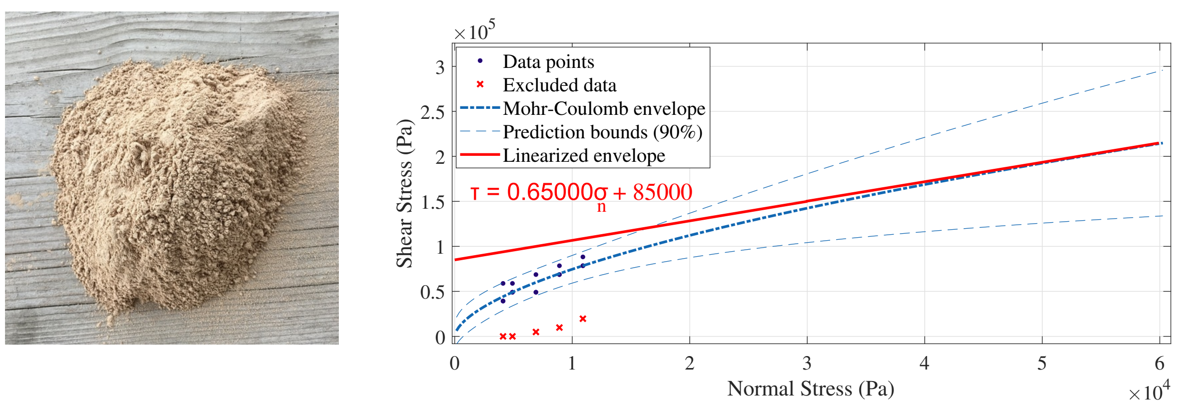

(a) *Dry clay of low plasticity. Expected $c = 86kPa$ and $27° \leq \phi \leq 35°$,*

(b) *Mohr-Coulomb envelope and linearization giving $c = 85kPa$ and $\phi = 33°$.*

Fig. 6: *Clay of low plasticity, compacted. Results give $c = 85kPa$ and $\phi = 33°$. Some data points overlap with each other.*

The tests gave a linearized envelopy showing a cohesion $c = 85kPa$ and an angle of internal friction $\phi = atan(0.6500) = 33.02°$. The initial Mohr-Coulomb curve is given by Eq.5 with the following coefficients (with 95% confidence bound) $a = 327.8(-312.6, 968.2)$, $b = 0.5892(0.3713, 0.8072)$ and $c = 0$. The goodness of fit for the non-linearized curve for dry clay is characterized by $R^2 = 0.7469$.

Next, compacted silt loam was tested. The sample was placed in a container and manually compacted by applying a load to the sample before the tests were conducted. Compacted silt loam has a cohesion of 60 to 90 kPa and an angle of internal friction between 25°and 32°. The results are presented in Fig.7.

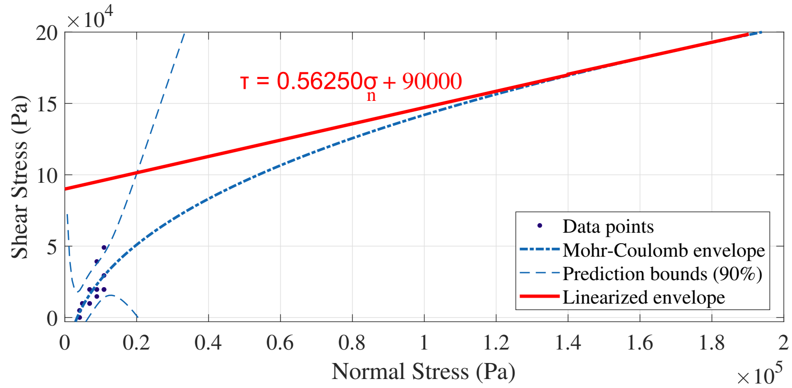

(a) Mohr-Coulomb envelope and linear approximation giving $c = 90kPa$ and $\phi = 29°$

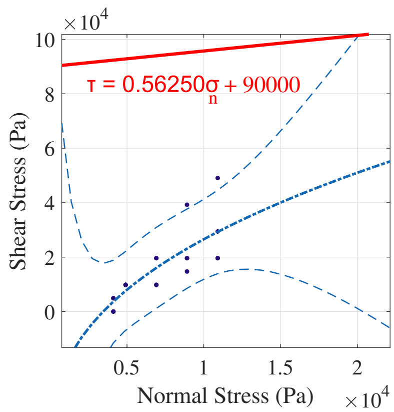

(b) Zoom on the part of the curve with data points.

(c) Silt Loam. Expected $c = 60 - 90kPa$ and $25° \leq \phi \leq 32°$.

Fig. 7: *Hand-held instrument tested in compacted silt loam. Results give $c = 90kPa$ and $\phi = 29°$. Some data points overlap with each other.*

The compacted silt loam led to the following results after linearization of the Mohr-Coulomb curve: $c = 90kPa$ and $\phi = atan(0.5625) = 29.36°$. The initial Mohr-Coulomb envelope is given by Eq.5 with the following coefficients (with 95% confidence bound) $a = 1960(-6.63e04, 7.022e04)$, $b = 0.3983(-2.671, 3.468)$ and $c = -5.027e04(-5.559e05, 4.554e05)$. The goodness of fit for the non-linearized curve for compacted silt loam is characterized by $R^2 = 0.6234$.

The third sample material tested was well graded, fine grain, cohesionless sand with an expected angle of internal friction ranging between 36°and 41°.

(a) Fine grain, well graded sand. Expected $c = 0kPa$ and $36° \leq \phi \leq 41°$

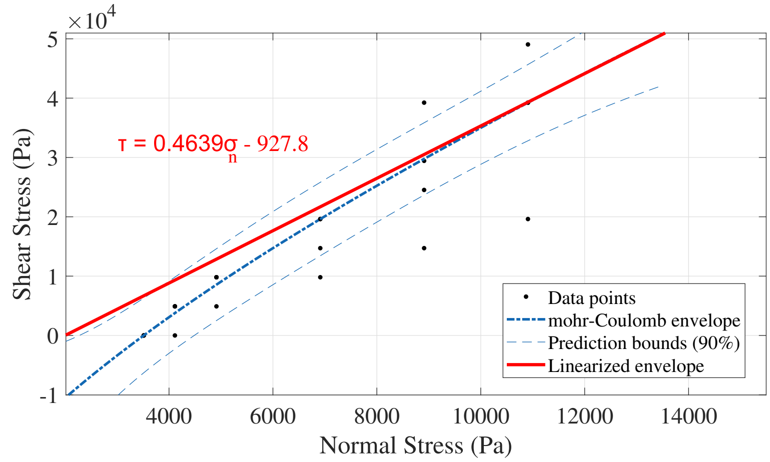

(b) Mohr-Coulomb envelope and linear approximation giving $c = -0.92kPa$ and $\phi = 25°$

Fig. 8: *Tests of the hand-held shear vane in fine grain sand material of known parameters.*

The results show a tangent with a slope (i.e., cohesion) $c = -0.9278kPa$ and an angle of internal friction $\phi = atan(0.4639) = 24.88°$ for fine, well graded sand. The Mohr-Coulomb curve before linearization is given by Eq.5 with the following coefficients (with 95% confidence bound) $a = 102.7(-639.8, 845.2)$, $b = 0.7039(-0.003083, 1.411)$ and $c = -3.217e04(-8.106e04, 1.671e04)$. The goodness of fit for the non-linearized envelope for fine, well graded sand is characterized by $R^2 = 0.9463$.

6.2. Hand-held pocket shear vane: field testing

Two tests were conducted in the field. A sand pit under dry conditions was chosen, where the cohesion is expected to be $0kPa$ (cohesionless) and the angle of internal friction is usually between 37°and 38°for such material. The results are presented in Fig.9b, where the resulting Mohr-Coulomb envelope is shown.

(a) Sand pit in which tests were performed. Expected values are $c = 0kPa$ and $\phi = 37° - 38°$.

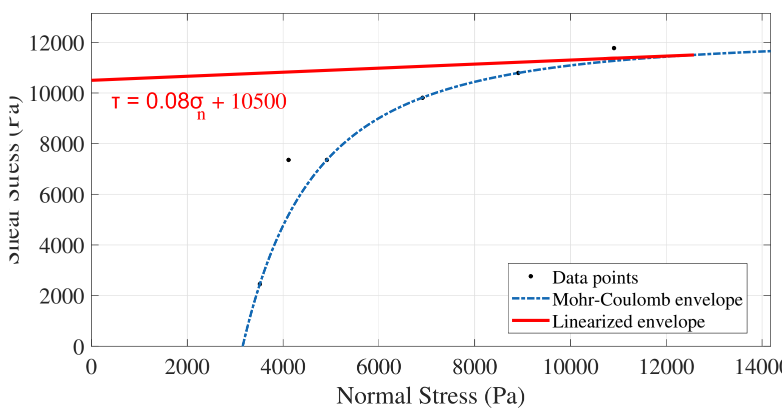

(b) Mohr-Coulomb envelope and linear approximation giving $c = 10.5kPa$ and $\phi = 4.57°$

Fig. 9: *Test of the hand-held pocket shear vane in cohesionless sand under dry conditions.*

From the plotted data in Fig.9, the retrieved cohesion from the linearized Mohr-Coulomb envelope is $c = 10.5kPa$ and the angle of internal friction is $\phi = atan(0.0800) = 4.57°$. The initial Mohr-Coulomb curve is given by Eq.5 with the following coefficients (with 95% confidence bound) $a = -2.615e11, (-5.793e12, 5.27e12)$, $b = -2.095(-4.723, 0.5321)$ and $c = 1.217e04(7598, 1.675e04)$ The goodness of fit of the Mohr-Coulomb envelope is characterized by $R^2 = 0.9652$

The second experiment was conducted in saturated silt loam. The results are presented in Fig.10.

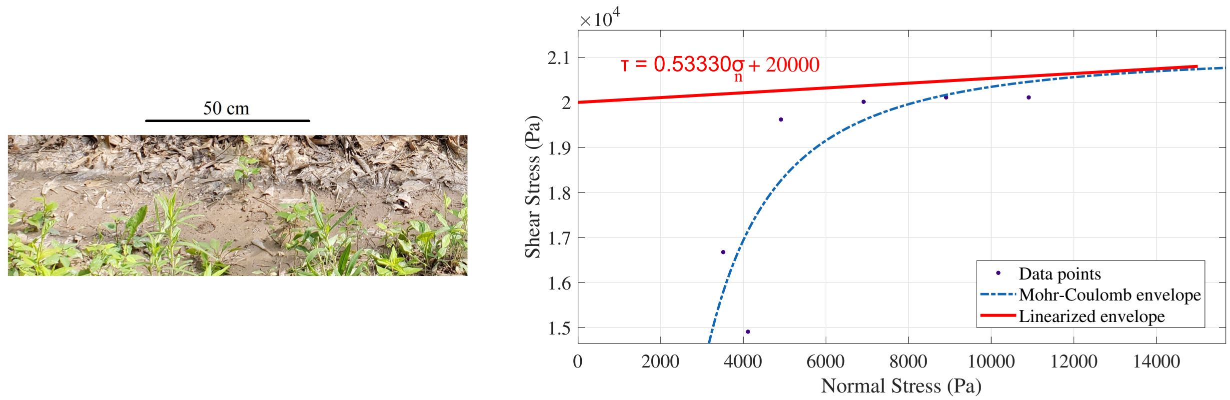

(a) *Saturated silt loam, expected $c = 10kPa - 20kPa$ and $\phi = 25° - 32°$*

(b) *Mohr-Coulomb envelopes and linear approximation giving $c = 20kPa$ and $\phi = 28°$.*

Fig. 10: *Hand-held instrument tested on saturated Silt Loam, with geological unit being quaternary alluvial mix of mostly silt mixed with fine sand and clay.*

The retrieved cohesion from Fig.10 is $c = 20kPa$ and friction angle is $\phi = atan(0.5333) = 28.07°$. The Mohr-Coulomb curve is given by Eq.5 with the following coefficients (with 95% confidence bound) $a = -2.544e10(-2.006e12, 1.955e12)$, $b = -1.885(-11.6, 7.829)$ and $c = 2.108e04(1.007e04, 3.209e+04)$. The goodness of fit of the Mohr-Coulomb envelope for this test is characterized by $R^2 = 0.6821$.

Table 2: Results of cohesion c and angle of internal friction ϕ from testing (hand-held instrument) compared to expected values (Obrzud, 2010; MnDOT, 2007). In green are adequate results, and in red, inadequate results.

Description	USCS	Expected c (kPa)	Measured c (kPa)	Expected ϕ (°)	Measured ϕ (°)
Controlled samples					
Clay of low plasticity, compacted	CL	86	85	27 − 35	33
Silt loam, compacted	ML, OL, MH, OH	60 − 90	90	25 − 32	29
Sand, fine grain, well graded	SW, SP	0	-1	36 − 41	25
Field testing					
Sand	SP	0	10.5	37 − 38	4.9
Silt loam, saturated	ML, OL, MH, OH	10 − 20	20	25 − 32	28

6.3. Interpretation of results

The results are summarized in Table 2. Overall, the tests give a accurate cohesion and angle of internal friction (within the expected range for the material). The exceptions to the rule are the sand samples, that give a negative cohesion in one case and an unrealistic angle of internal friction in the other. This shows that the proposed method is limited to cohesive soils (known to be present on Mars (Sullivan et al., 2011)). For the mounted pocket shear vane, cohesionless soil testing was therefore eliminated.

6.4. Mounted pocket shear vane: controlled samples

The mounted pocket shear vane has been tested in compacted clay of low plasticity. The results are presented in Fig.11. The payload prototype currently takes between 3 to 5 minutes for each measurement(the low linear servo precision requires a very slow pace to adjust weights accurately), and 25 measurements total were taken to construct the Mohr-Coulomb curve (five for each mass tested, 100g to 500g in 100g increments). Due to the unpredictability of field testing, results that are known to be unrealistic are omitted from the data. For example, when the instrument was not properly deployed (such as tilted, not touching the ground evenly, etc...) the resulting data were not considered.

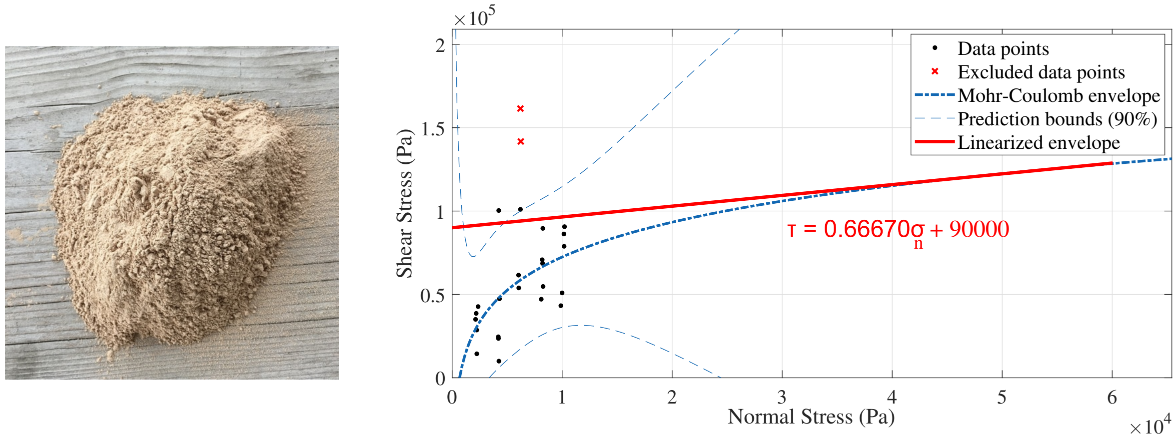

(a) *Dry clay of low plasticity. Expected $c = 86kPa$ and $27° \leq \phi \leq 35°$,*

(b) *Mohr-Coulomb envelope and linearization giving $c = 90kPa$ and $\phi = 34°$.*

Fig. 11: *Mounted instrument tested in Clay of low plasticity, compacted. Results give $c = 90kPa$ and $\phi = 34°$. Some data points overlap with each other, while others were eliminated due to being .*

The retrieved cohesion is $c = 90kPa$ and the angle of internal friction is $\phi = atan(0.6667) = 33.69°$. Unlike the tests with the hand-held instruments, the data for the mounted pocket shear vane are more widespread, leading to a goodness of fit for the non-linearized curve characterized by $R^2 = 0.3466$. The variables values for Eq.5 are the following (with a 95% confidence bound): $a = 2.338e + 05(-1.601e + 07, 1.648e + 07)$, $b = 0.06755(-2.917, 3.052)$ and $c = -3.632e + 05(-1.866e + 07, 1.794e + 07)$. The estimated maximum power consumption is 83.056 W, and the total power consumption of the payload per data collection should not exceed 2.5 kJ. These values do not include the resources expended to transition the rover from a driving stance to a squat in order to conduct the experiment, or the minute movement needed to position the mounted pocket shear vane over fresh soil for a new measurement.

6.5. Mounted pocket shear vane: field testing

Field testing was conducted in saturated silt loam, with 15 data points taken (three for each mass from 100g to 500g). The retrieved cohesion is $c = 20kPa$ and angle of internal friction is $\phi = atan(0.4333) = 23.43°$. Unlike the hand-held experiments, a lot of points had to be eliminated because the position of the instrument led to false readings. The goodness of fit for the non-linearized curve is characterized by $R^2 = 0.8938$. The variables values for Eq.5 are the following (with a 95% confidence bound): $a = 2.338e + 05(-1.601e + 07, 1.648e + 07)$, $b = 0.06755(-2.917, 3.052)$ and $c = -3.632e + 05(-1.866e + 07, 1.794e + 07)$.

6.6. Interpretation of results

The mounted pocket shear vane appears to be extremely sensitive to its tilt and gives false results when operating at an angle, which affected mostly field testing. The overall results are presented in Table 3. The

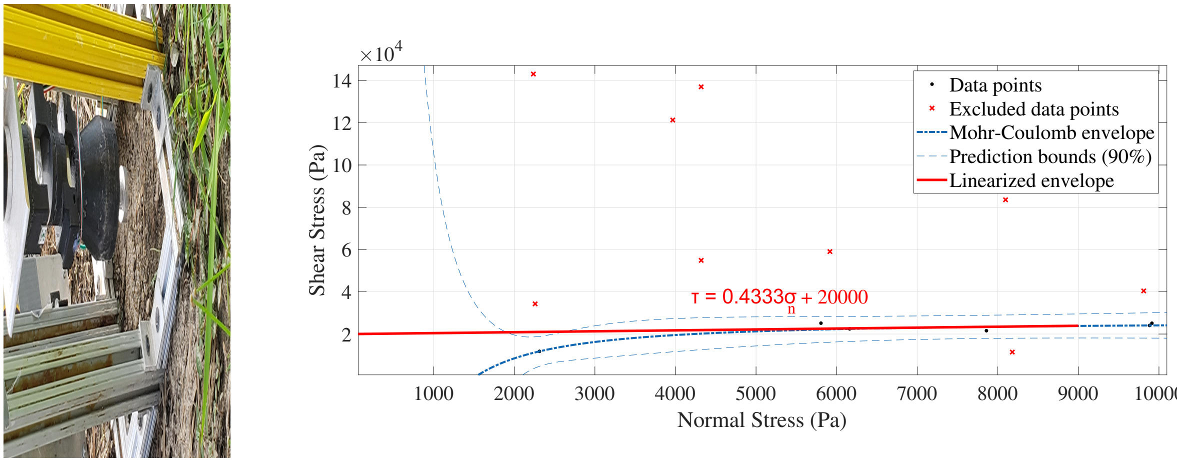

(a) *Silt loam, saturated. Expected $c = 10 - 20kPa$ and $25° \leq \phi \leq 32°$,*

(b) *Mohr-Coulomb envelope and linearization giving $c = 20kPa$ and $\phi = 23.5°$.*

Fig. 12: *Mounted instrument tested in Silt loam, saturated (in-situ). Results give $c = 20kPa$ and $\phi = 24°$. Some data points overlap with each other, while others were eliminated.*

Table 3: Results of cohesion c and angle of internal friction ϕ from testing (mounted pocket shear vane) compared to expected values (Obrzud, 2010; MnDOT, 2007). In green are adequate results.

Description	USCS	Expected c (kPa)	Measured c (kPa)	Expected ϕ (°)	Measured ϕ (°)
Controlled samples					
Clay of low plasticity, compacted	CL	86	90	27 − 35	34
Field testing					
Silt loam, saturated	ML, OL, MH, OH	10 − 20	20	25 − 32	23.5

values are not as close to the expected parameters as they were with the hand-held instrument, due to the mounted pocket shear vane being significantly affected by testing conditions (e.g., tilt). Some of the resulting outputs are a little out of range (e.g., cohesion of $90kPa$ instead of $86kPa$), but the difference being less than 5% of the actual value, it is negligible.

7. Discussion and future work

As seen with the hand-held experiments, the modified pocket shear vane leads to results that can be used to compute parameters of soils with a non-zero cohesion. When mounted, the instrument performs adequately on flat terrain, and is capable of giving intrinsic parameters needed to identify a terrain. The pocket shear vane's ease of use, its light weight and compact form makes it a perfect candidate for planetary surface missions.

The transition to remote operation shows that many improvements can be made to the mounted instrument. One way to improve its operation involves selecting components that are better suited for such a design. For instance, the current linear servo struggled to precisely apply axial load, especially at weights higher than 3 kg. A lead screw and stepper motor would be able to apply force more precisely than the potentiometer-based linear servo. Also due to lack of linear servo precision in the current prototype, it was witnessed that the device performed better under light loads (for masses between 100 - 500g). In the future, utilizing more sensitive load cells that have a maximum weight closer to the light loads used in the experiment will greatly increase the accuracy of individual measurements. It should be noted that the prototype shown in this paper is a proof of concept, and the device performance will be improved in the next version by utilizing higher quality components that will increase stiffness and precision of the overall mechanism.

In addition to improving on the current design to obtain more accurate results, future work includes testing under a wider range of conditions, as well as developing an algorithm to automatically interpret the results and compute the cohesion and angle of internal friction on board. Additionally, this instrument will be mounted on a physical robot currently under construction at the Interactive Robotics Laboratory at West Virginia University, and further testing will be conducted with the shear vane fully integrated. This research will also lead to studying other types of instrument, to be able to predict soil parameters in cohesionless terrain.

Acknowledgement

This research is supported by NASA EPSCoR Research Cooperative Agreement WV-80NSSC17M0053 and the Benjamin M. Statler fellowship.

References

Arora, A., Fitch, R., & Sukkarieh, S. (2017). An approach to autonomous science by modeling geological knowledge in a bayesian framework. In *2017 IEEE/RSJ International Conference on Intelligent Robots and Systems (IROS)* (pp. 3803–3810). IEEE.

Bajracharya, M., Maimone, M. W., & Helmick, D. (2008). Autonomy for mars rovers: Past, present, and future. *Computer*, *41*, 44–50.

Biesiadecki, J. J., Leger, P. C., & Maimone, M. W. (2007). Tradeoffs between directed and autonomous driving on the mars exploration rovers. *The International Journal of Robotics Research*, *26*, 91–104.

Bishop, A. W., & Henkel, D. J. (1962). The measurement of soil properties in the triaxial test, .

Brooks, C. A., & Iagnemma, K. (2005). Vibration-based terrain classification for planetary exploration rovers. *IEEE Transactions on Robotics*, *21*, 1185–1191.

Candela, A., Thompson, D., Dobrea, E. N., & Wettergreen, D. (2017). Planetary robotic exploration driven by science hypotheses for geologic mapping. In *2017 IEEE/RSJ International Conference on Intelligent Robots and Systems (IROS)* (pp. 3811–3818). IEEE.

Chhaniyara, S., Brunskill, C., Yeomans, B., Matthews, M., Saaj, C., Ransom, S., & Richter, L. (2012). Terrain trafficability analysis and soil mechanical property identification for planetary rovers: A survey. *Journal of Terramechanics*, *49*, 115–128.

Gaines, D., Anderson, R., Doran, G., Huffman, W., Justice, H., Mackey, R., Rabideau, G., Vasavada, A., Verma, V., Estlin, T. et al. (2016). Productivity challenges for mars rover operations, .

Gellert, R., Campbell, J., King, P., Leshin, L., Lugmair, G., Spray, J., Squyres, S., & Yen, A. (2009). The alpha-particle-x-ray-spectrometer (apxs) for the mars science laboratory (msl) rover mission. In *The 40th Lunar and Planetary Science Conference, LPI Contribution* (p. 2364). volume 1468.

Giacoboni, N. (2020). Basic custom arduino library for hx711. URL: `https://www.mathworks.com/matlabcentral/fileexchange/66641-basic-custom-arduino-library-for-hx711`.

Girdhar, Y., & Dudek, G. (2016). Modeling curiosity in a mobile robot for long-term autonomous exploration and monitoring. *Autonomous Robots*, *40*, 1267–1278.

Golombek, M., Otero, R., Heverly, M., Ono, M., Williford, K., Rothrock, B., Milkovich, S., Almeida, E., Calef, F., Williams, N. et al. (2017). Characterization of mars rover 2020 prospective landing sites leading up to the second downselection. In *Lunar and Planetary Science Conference*. volume 48.

Golombek, M., & Rapp, D. (1996). Size-frequency distributions of rocks on mars. In *Lunar and Planetary Science Conference*. volume 27.

Hedrick, G., Ohi, N., & Gu, Y. (2020). Terrain-aware path planning and map update for mars sample return mission. *IEEE Robotics and Automation Letters*, *5*, 5181–5188.

Helmick, D., Angelova, A., Matthies, L., Brooks, C., Halatci, I., Dubowsky, S., & Iagnemma, K. (2008). Experimental results from a terrain adaptive navigation system for planetary rovers. In *the Ninth International Symposium on Artificial Intelligence, Robotics and Automation in Space, i-SAIRAS*.

Iagnemma, K., Kang, S., Brooks, C., & Dubowsky, S. (2003). Multi-sensor terrain estimation for planetary rovers. In *Proceedings of the 8th international symposium on artificial intelligence, robotics, and automation in space. IEEE Press, New York*.

Ishigami, G., Nagatani, K., & Yoshida, K. (2007). Path planning for planetary exploration rovers and its evaluation based on wheel slip dynamics. In *Proceedings 2007 IEEE International Conference on Robotics and Automation* (pp. 2361–2366). IEEE.

Ishigami, G., Nagatani, K., & Yoshida, K. (2011). Path planning and evaluation for planetary rovers based on dynamic mobility index. In *2011 IEEE/RSJ International Conference on Intelligent Robots and Systems* (pp. 601–606). IEEE.

Klein, E., Nilsen, E., Nicholas, A., Whetsel, C., Parrish, J., Mattingly, R., & May, L. (2014). The mobile mav concept for mars sample return. In *2014 IEEE Aerospace Conference* (pp. 1–9). IEEE.

Labuz, J. F., & Zang, A. (2012). Mohr–coulomb failure criterion. *Rock mechanics and rock engineering*, *45*, 975–979.

Melosh, H. J. (2011). *Planetary surface processes* volume 13. Cambridge University Press.

MEPAG, N. D. S. A. G. (2008). Science priorities for mars sample return.

MnDOT (2007). *MnDOT Pavement Design Manual*.

Obrzud, R. (2010). *The hardening soil model: A practical guidebook*. Zace Services.

Ojeda, L., Borenstein, J., Witus, G., & Karlsen, R. (2006). Terrain characterization and classification with a mobile robot. *Journal of Field Robotics*, *23*, 103–122.

Ono, M., Rothrock, B., Almeida, E., Ansar, A., Otero, R., Huertas, A., & Heverly, M. (2016). Data-driven traverability analysis for mars 2020 landing site selection, .

Papadakis, P. (2013). Terrain traversability analysis methods for unmanned ground vehicles: A survey. *Engineering Applications of Artificial Intelligence*, *26*, 1373–1385.

Rahmatian, L. A., & Metzger, P. T. (2010). Soil test apparatus for lunar surfaces. In *Earth and Space 2010: Engineering, Science, Construction, and Operations in Challenging Environments* (pp. 239–253).

Rothrock, B., Kennedy, R., Cunningham, C., Papon, J., Heverly, M., & Ono, M. (2016). Spoc: Deep learning-based terrain classification for mars rover missions. In *AIAA SPACE 2016* (p. 5539).

Schroeder, C. (2019). Life on mars: my 15 amazing years with oppy, nasa's record-breaking rover, .

Sullivan, R., Anderson, R., Biesiadecki, J., Bond, T., & Stewart, H. (2011). Cohesions, friction angles, and other physical properties of martian regolith from mars exploration rover wheel trenches and wheel scuffs. *Journal of Geophysical Research: Planets*, *116*.

Witze, A. (2014). Nasa plans mars sample-return rover. *Nature News*, *509*, 272.

Zacny, K., Wilson, J., Craft, J., Asnani, V., Oravec, H., Creager, C., Johnson, J., & Fong, T. (2010). Robotic lunar geotechnical tool. In *Earth and Space 2010: Engineering, Science, Construction, and Operations in Challenging Environments* (pp. 166–181).

Zoback, M. D. (2010). *Reservoir geomechanics*. Cambridge University Press.